Chinese Chemical Letters 33 (2022) 2129–2133

Contents lists available at ScienceDirect

Chinese Chemical Letters

journal homepage: www.elsevier.com/locate/cclet

Enhanced heterogeneous activation of peroxymonosulfate by boosting internal electron transfer in a bimetallic Fe_3O_4-MnO_2 nanocomposite

Qingqing Shi[a], Shengyan Pu[a,b,*], Xi Yang[a], Peng Wang[a], Bo Tang[a], Bo Lai[c]

[a] State Key Laboratory of Geohazard Prevention and Geoenvironment Protection, Chengdu University of Technology, Chengdu 610059, China
[b] Department of Civil and Environment Engineering, Hong Kong Polytechnic University, Hong Kong, China
[c] State Key Laboratory of Hydraulics and Mountain River Engineering, College of Architecture and Environment, Sichuan University, Chengdu 610065, China

ARTICLE INFO

Article history:
Received 29 April 2021
Revised 11 June 2021
Accepted 28 July 2021
Available online 5 August 2021

Keywords:
Bimetallic oxides
Peroxymonosulfate
Sulfate radical
Synergism effects
Redox species cycle

ABSTRACT

Transition metal-based bimetallic oxides can effectively activate peroxymonosulfate (PMS) for the degradation of organic contaminants, which may be attributed to the enhanced electron transfer efficiency between transition metals. Here, we investigated the high-efficiency catalytic activation reaction of PMS on a well-defined bimetallic Fe-Mn nanocomposite (BFMN) catalyst. The surface topography and chemical information of BFMN were simultaneously mapped with nanoscale resolution. Rhodamine B (RhB, as a model pollutant) was used to evaluate the oxidation activity of PMS activation system. The maximum absorption peak of RhB obviously blue shifted from 554 nm to 501 nm, and decreased sharply to disappear completely within 60 min. The removal performance is better than most of the reported single transition metal oxide. X-ray photoelectron spectroscopy (XPS) imaging of the BFMN electronic structure after catalytic activation confirmed that the accelerated internal electron transfer is mainly caused by the synergy effect of Mn and Fe sites at the catalysis boundary. The outstanding ability of BFMN for PMS chemical adsorption and activation may attribute to the enhanced covalency and reactivity of Mn-O. These results of this study can advance understandings on the origins of bimetallic oxides activity for PMS activation and developing the efficient metal oxide catalysts in real practice.

Iron and manganese are the two most abundant metal elements in the earth's crust. Due to these advantages of low cost, high environmental compatibility and multivalent, they are often used as catalysts in environmental remediation processes [1,2]. As shown in Table S1 (Supporting information), the insufficient degradation efficiency of heterogeneous peroxymonosulfate (PMS) system by single-metal catalyst for the degradation of organic compounds usually need longer reaction time. To a certain extent, the practical application of this technology is limited by various reasons [3,4]. Therefore, the development of an efficient and recyclable catalyst is necessary for the PMS activation technology [5,6]. More recently, iron-based bimetallic oxides with higher catalytic reactivity and stability have been proposed as the promising activators for PMS heterogeneous activation systems. The favorable synergistic effects were mainly attributed to the generation of defects, high degree of dispersion and redox interaction [7,8]. The binary metal structure formed by the junction of Fe_3O_4 and MnO_2 was proposed as an effective method to enhance the removal efficiency and reusability. The generation of reactive oxygen species (ROS), such as sulfate radicals ($SO_4^{\bullet-}$), hydroxyl radicals ($HO^{\bullet}$) and singlet oxygen ($^1O_2$), were determined from the system of heterogeneous activation PMS by bimetallic oxides [9,10]. Nano Fe_3O_4 has high magnetic properties, which can be separated from water by magnetic field and often used for PMS activation [11,12].

The mechanism of PMS activated by Fe-Mn bimetallic catalyst to generate ROS has recently been established [13,14]. However, whether the degradation process of organic pollutants in the system occurs mainly in the solution or on the surface of the bimetallic catalyst [15,16] was not clear. Surprisingly, transition metals such as Mn and Cu have a thermodynamic inhibitory effect on the direct oxidation of PMS, but it may still occur in some metal oxide/PMS systems [17,18]. Recent studies have found that the catalytic activity of transition metal oxides is positively related with the degree of covalency of transition metal-O, which is supported by the enhanced hybridization between the transition metal 3d and O 2p orbitals [19,20]. How to accelerate the efficient redox cycling of transition metal [21,22] and break the thermodynamic limit between the covalency of transition metal-O in the catalyst and the transition metal? The oxidation conversion capacity of the generated ROS in the system needed to be further evaluated. These

* Corresponding author.
E-mail address: pushengyan13@cdut.edu.cn (S. Pu).

https://doi.org/10.1016/j.cclet.2021.07.063
1001-8417/

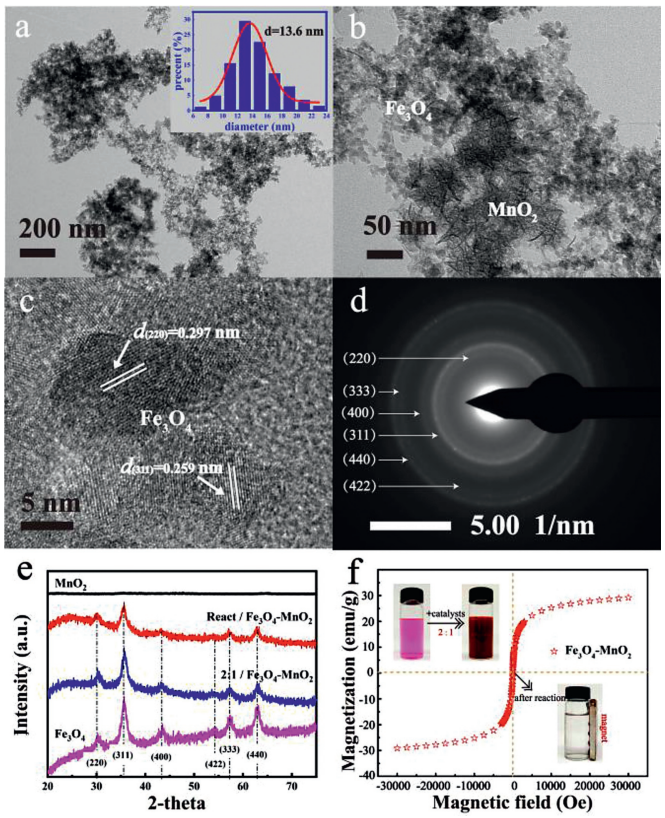

Fig. 1. TEM of BFMN (a) and (b) mixture of Fe_3O_4 and MnO_2, (c) HRTEM (images inset means distribution of BFMN size (obtained by counting 300 particles)), (d) SEAD pattern, (e) XRD spectrum and (f) hysteresis loop of BFMN [n(Fe):n(Mn) = 2:1].

interesting questions still unknown and deserve further study to understanding the intrinsic origin of the innovative transition metals oxide activity.

To address these major knowledge gaps, a novel bimetallic Fe_3O_4-MnO_2 nanocomposite (BFMN) configuration were synthesized by using Fe_3O_4 particle as substrate to load MnO_2. The catalytic performance and stability of the as-prepared BFMN in catalytic PMS activation was evaluated in details by its ability to degrade Rhodamine B (RhB, as a model organic contaminants), and the catalytic and synergistic effect mechanism were also investigated. Our findings will help to understand and re-evaluate the intrinsic origin cause of the superior activity of bimetallic synergy on PMS activation.

The BFMN sample exhibited similar flocculent nanocomposite (*ca.* 13.6 ± 2.0 nm) (Fig. 1a), distinct from the physically mixed of pure MnO_2 (rod-like) and Fe_3O_4 (flocculent) nanoparticles in Fig. 1b. The lattice fringes with spaces of 0.297 nm and 0.259 nm can be clearly observed by high resolution transmission electron microscopy (HRTEM) image (Fig. 1c), which showed a good spacing between adjacent lattice fringes of BFMN. The result corresponded to the (220) and (311) crystal planes of Fe_3O_4 [7]. Furthermore, the crystal faces of catalyst were also reflected by the selected area electron diffraction (SEAD) patterns (Fig. 1d). The crystal structure (Fig. 1e) of the prepared catalyst after the reaction had little change, which also confirmed the good stability of BFMN. These results implied that the nanocomposites have been successfully synthesized. As shown in Fig. 1f and Fig. S1 (Supporting information), the BFMN exhibited an extremely magnetic recovery potential and the relative content of Fe_3O_4 could affect the magnetic induction.

Considering a rapid analysis processing of samples through spectrophotometric measurement, RhB was used to explore the catalytic activities of BFMN for PMS activation in this study. Before adding PMS to the reaction system, the pre-equilibrium experiment between RhB and the catalyst was performed to eliminate the adsorption and degradation of PhB by the catalyst. Previous studies reported that the catalysts with manganese oxide can slightly oxidize RhB [23]. This process resulted in a different blue shift of the UV absorption spectrum of RhB before the catalytic activation reaction in Figs. 2a-c. After adding PMS, the absorption spectra of RhB changed drastically in Fe_3O_4, MnO_2 and BFMN-activated PMS systems. As shown in Fig. 2a, only a weak decrease of the intensity of the RhB peaks and slight blue shift were observed in Fe_3O_4-activated PMS. Interestingly, a blue shift of the maximum absorption band of RhB from 554 nm to 501 nm was observed in MnO_2-activated PMS system. The maximum absorption wavelength decreased sharply within 15 min, and slightly change after 25 min (Fig. 2b). Notably, the maximum absorption wavelength in BFMN-activated PMS system has also been rapidly blue-shifted from 554 nm to 501 nm, and a solution with green fluorescence is rapidly formed. Compared with the MnO_2 active system with similar phenomena, the higher efficiency decolorization RhB (above 90% within 2 min) was possessed and accompanied by a faster degradation reaction (almost 100% within 60 min) in the BFMN-activated PMS (Fig. 2c).

The degradation efficiency of RhB in the activated PMS system were further accurately evaluated through the evolution of the UV-vis spectrum. As shown in Fig. S2 (Supporting information), over 98% degradation efficiency can reach and more than 90% TOC removal can be accomplished in BFMN-activated PMS system within 15 min (Fig. S2b), which is much higher than that of pure PMS (11%), Fe_3O_4/PMS (30%) and MnO_2/PMS (68%) system under similar conditions (the data is not displayed). The order of the apparent rate constant (K_{app}) by apparent pseudo first-order kinetic model was BFMN (0.264, 0.227 and 0.167 min^{-1} for n[Fe]:n[Mn] = 1:1, 2:1 and 3:1, respectively) > MnO_2 (0.061 min^{-1}) > Fe_3O_4 (0.034 min^{-1}) > PMS (K_{app} = 0.006 min^{-1}). The superior activity of BFMN for PMS activation and its application potential in the environment are further verified through using more complex and real water samples. As shown in Fig. S3 (Supporting information), the BFMN system still achieved more than 90% RhB degradation within 15 min for treating tap water and surface water. The mineralization of RhB in tap water and surface water were 53% and 39%, respectively. These results indicated that BFMN activated PMS system showed a significant advantage in degradation and mineralization capability for RhB.

The apparent rate constant (k_{app}) of RhB degradation obviously increased from 0.006 min^{-1} to 0.157 min^{-1} with the increasing of BFMN dosage from 0 to 0.3 g/L (Fig. S4a in Supporting information). The adequate BFMN might provide more active sites for activating PMS. However, when the dosage of BFMN increased from 0.3 g/L to 0.35 g/L, a prominent decrease of the k_{app} value from 0.157 min^{-1} to 0.129 min^{-1} was observed. The radicals at high concentration may undergo self-quenching, which also prohibit a continuous increase of $SO_4^{\bullet-}$ [24]. The k_{app} values almost linearly increased from 0.013 min^{-1} to 0.166 min^{-1} as PMS dosage increased from 0 to 0.2 g/L (Fig. S4b in Supporting information). However, a prominent decrease of the k_{app} values with the increasing of PMS dosage (over 0.2 g/L) was observed. Excessive PMS can compete with RhB for ROS and adsorption sites [25], thereby limiting the degradation rate of RhB.

In addition, solution pH was an important reaction parameter for practical applications. As shown in Fig. S4c (Supporting information), the efficacy of BFMN-activated PMS was significantly affected by the solution pH from 3.0 to 11.0. A faster rate of RhB degradation with the k_{app} value of 0.160 min^{-1} was obtained at initial pH 5.6. In particular, the degradation rate of RhB is lower at the acidic pH (~3.0) solution. This result was mainly attributed to

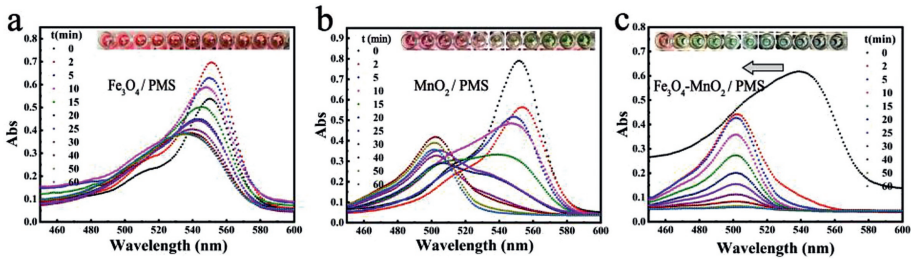

Fig. 2. Absorption spectrum of RhB degradation by Fe_3O_4, MnO_2, BFMN (n[Fe]:n[Mn] = 1:1), inset: color change during degradation. Reaction conditions: [catalysts] = 0.3 g/L, T = 25 °C, [RhB] = 20 mg/L, [PMS] = 0.3 g/L and initial pH 5.6.

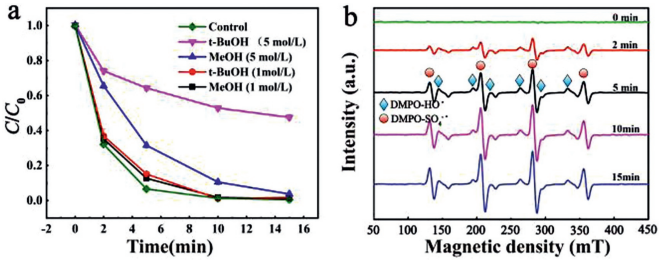

Fig. 3. (a) The effect of radical scavengers on RhB degradation in the BFMN/PMS system. (b) EPR spectra in activation of PMS under different time periods. Reaction conditions: [catalysts] = 0.3 g/L, T = 25 °C, [RhB] = 20 mg/L, [PMS] = 0.3 g/L and initial pH 5.6.

the stabilization effect of H^+ on PMS, which could stabilize PMS from being easily activated [25,26]. On the other hand, the pK_a value of RhB with cationic and zwitterionic forms is 3.7, and it mainly exists in the cationic form (RhB^+) in solutions lower than 3.7. A zwitterionic form ($RhB^{\pm}$) appeared pH values higher than 3.7 [27,28]. The weak electrostatic attraction is not enough to support its adsorption on the weakly electronegative BFMN surface. However, the RhB degradation was significantly inhibited with the increasing of initial pH over 5.6, the k_{app} value decreased from 0.160 min^{-1} to 0.052 min^{-1}. The phenomenon was usually ascribed to the increasing negative charge on the BFMN surface with the increasing of pH (Fig. S5 in Supporting information).

Additionally, the stability and reusability of BFMN catalyst were also evaluated. The catalyst was separated and collected using a magnet, and was simply regenerated by water wash before every experimental run. The efficiency of catalytic reaction system for RhB degradation after four times recycling runs (Fig. S6 in Supporting information) were slightly decreased. The weak reduction in degradation efficiency may be due to the loss of a small amount of catalyst during recovery (> 95%) and the reduction of the active site of the catalyst [29,30]. The result indicated that the prepared BFMN exhibited a good catalytic performance. Moreover, the metal leaching properties of the catalyst were also investigated. The concentration of leaching iron and manganese ions in the reaction system at different pH values were lower than the detection limit (0.03 mg/L and 0.01 mg/L, respectively), which further demonstrated the good stability of BFMN. The high stability and sustained activity of BFMN can be attributed to its unique structure and performance. Fe and Mn atoms with different valence were uniformly distributed in the BFMN nanocomposite crystal structure, and PMS can be activated at the same surface sites through a reversible redox process.

To identify the major radical active species involved in the RhB degradation, radical scavenging tests and EPR analysis using DMPO as a spin trap in BFMN/PMS system were conducted (Fig. 3). The degradation of RhB in BFMN-activated PMS system was obviously inhibited by the addition of *t*-BuOH (TBA, a $HO^{\bullet}$ quencher) and

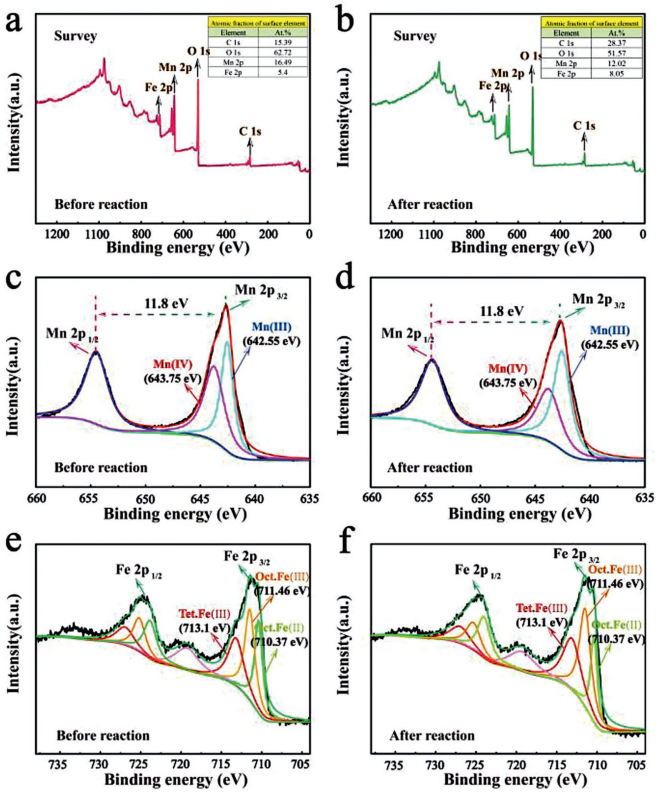

Fig. 4. XPS spectra of survey scan (a, b), Mn 2p (c, d) and Fe 2p (e, f) in BFMN before and after reactions.

EtOH (quencher for $HO^{\bullet}$ and $SO_4^{\bullet-}$). No free radical peaks were found in the alone PMS system without catalyst (Fig. 3b) [31]. After the addition of BFMN, a strong signal was obtained by the EPR spectra. The observed similar signals in the previous study could be assigned to DMPO-$SO_4^{\bullet-}$ and DMPO-$HO^{\bullet}$ adducts [7,18,32]. The higher signal intensity of $HO^{\bullet}$ than that of $SO_4^{\bullet-}$ was due to the fast transformation of DMPO-$SO_4^{\bullet-}$ to DMPO-$HO^{\bullet}$ adducts [33]. It should also be noted that the signal intensities of the free radical gradually increased with the RhB degradation within 15 min (Fig. 3b). These results indicated that the generated $HO^{\bullet}$ and $SO_4^{\bullet-}$ were mainly responsible for the RhB degradation.

The catalysis of BFMN predominantly involves a series of surface-based reactions, which is supported by the negligible RhB degradation in the homogeneous control with resemble the leaching Fe and Mn ions in bulk solution (Fig. S7 in Supporting information). The surface-based reactions can be fundamentally affected by the electronic structure of the catalyst surface. The specific valent state distribution of both Fe and Mn of BFMN before and after the reaction were examined by using X-ray photoelectron spectroscopy (XPS) spectra. As depicted in Fig. 4, the detailed deconvo-

lutions of XPS Mn 2p spectrum of fresh BFMN catalyst concluded a spin-orbit bimodal of Mn $2p_{1/2}$ and Mn $2p_{3/2}$ with a binding energy gap of 11.8 ± 0.1 eV. Only one peak in Mn $2p_{3/2}$ spectrum at 643.75 eV was assigned to Mn(IV) [34-36]. After the catalytic reaction, a significant peak shift to a higher binding energy can be observed. The deconvoluted Mn $2p_{3/2}$ spectrum of BFMN with two peaks at binding energies 643.75 and 642.55 eV, corresponding to the Mn(IV) and Mn(III), respectively. The 57.9% drop of the Mn(IV) content in BFMN after reaction was converted to Mn(III). It was indicated that Mn(IV) species played a critical catalytic role in the reaction, consistent with previous reports [19,37]. This mutual conversion confirmed that the process of PMS activation was accompanied by redox conversion among different Mn species Eqs. 2-5.

The intrinsic catalytic effect of Mn species in BFMN is mainly due to the hybridization between Mn 3d and O 2p orbitals. The high catalytic activity from the enhancing the interaction between catalysts and PMS could be accounted by the strong overlap between Mn e_g and O p orbitals. The strong orbital overlap between Mn e_g and O p orbitals could enlarge the covalency of Mn-O and dominate the Fe-Mn synergy in boosted PMS activation [38,39]. Moreover, the surface hydroxyl groups of MnO_2 are abundant in the aqueous solution [40] and can react with PMS to produce $SO_4^{\bullet-}$ for degradation of the organic contaminants [41]. Specifically, Mn(IV) ($e_g = 0$) is more prone to binding and adsorbing PMS over Mn(II) ($e_g = 2$) and Mn(III) ($e_g = 1$), which enable to increase the cyclic reaction rate of effectively realize Mn(IV)/Mn(III) recycling and further activate PMS [19].

Unlike the Mn species, as for the Fe $2p_{3/2}$ spectra of used BFMN samples, three peaks can be deconvoluted into with binding energies of 710.4, 711.5 and 713.1 eV, which were assigned to octahedral Fe(II), octahedral Fe(III) and tetrahedral Fe(III), respectively. According to deconvolution of Fe 2p envelop, the octahedral Fe(II) was significantly decreased (30.6% → 21.4%) and the octahedral Fe(III) was slightly increased (38.2% → 43.2%). Only 4.2% of the tetrahedral Fe(III) were converted from to octahedral Fe(III) and tetrahedral Fe(III) after reacting with PMS, which suggested electron transfer from Fe(II) species. The transition metal species could play an important role for effective PMS activation Eqs. 1 and 8 and the generation of reactive radicals accompanied with the rapid redox cycles of Mn(IV)/Mn(III) [42,43]. The formed bimetal composite crystal structure of BFMN could facilitate the electrons transfer across the atomic interface.

Based on the stated above, a synergistic effect between Fe and Mn oxides in the PMS activation process could be proposed. The addition of Mn in the complex catalyst played a vital role in the process of activating PMS for pollutants degradation. Previous studies believed that the direct electron transfer between Fe and Mn in BFMN is the most important synergism for PMS activation [32,44]. The continuous ligand promotes the partial reduction of Mn(IV), which leads to the migration of Mn atoms from the edge to the interlayer. The vacancy of the non-specific octahedron is blocked and the side edge sites are activated, thereby achieving excellent selectivity for PMS activation. Recent research has identified the key role of Mn-O covalency in bimetallic catalysts, which points to a long-overlooked approach to the synergy between transition metals [19]. In the multiple reaction step Eqs. 1-12, only Mn(IV) reduction (Eq. 1) is thermodynamically unfavorable because the redox potential of Mn(IV)/Mn(III) (0.95 V) is relatively lower than that of $SO_5^{\bullet-}/HSO_5^-$ (1.1 V) (Table S2). However, the Mn(IV) (57.9%) was significantly reduced in our system, which could mainly attribute to the increase of Mn-O covalency. Specifically, the introduction of Fe leads to an increasing in the covalency of Mn-O, giving Mn(IV) a stronger ability to pull electrons out of oxygen [45]. The result increased the oxidability of Mn species and the actual redox potential, thus breaking the thermodynamic limit of Mn(IV) reduction by O species. It has been confirmed that the increased Mn-O covalency mainly promotes catalytic activity by reducing the charge transfer energy between Mn and O species [19]. In general, the interaction between Fe and Mn in BFMN leads to an increase in the Mn-O covalency, which in turn accelerates the charge transfer between Mn and O, thereby promoting the activation of PMS.

$$\equiv Mn(IV) + HSO_5^- \rightarrow \equiv Mn(III) + SO_5^{\bullet-} + H^+ \quad (1)$$

$$\equiv Mn(III) + HSO_5^- \rightarrow \equiv Mn(IV) + SO_4^{\bullet-} + OH^- \quad (2)$$

$$\equiv Fe(II) + HSO_5^- \rightarrow \equiv Fe(III) + SO_4^{\bullet-} + OH^- \quad (3)$$

$$\equiv Mn(III) + HSO_5^- \rightarrow \equiv Mn(IV) + SO_4^{2-} + HO^{\bullet} \quad (4)$$

$$\equiv Fe(II) + HSO_5^- \rightarrow \equiv Fe(III) + SO_4^{2-} + HO^{\bullet} \quad (5)$$

$$SO_4^{\bullet-} + H_2O \rightarrow SO_4^{2-} + HO^{\bullet} + H^+ \quad (6)$$

$$SO_4^{\bullet-} + OH^- \rightarrow SO_4^{2-} + HO^{\bullet} \quad (7)$$

$$\equiv Fe(III) + HSO_5^- \rightarrow \equiv Fe(II) + SO_5^{\bullet-} + H^+ \quad (8)$$

$$SO_4^{\bullet-}/HO^{\bullet} + RhB \rightarrow \text{intermediates} \rightarrow CO_2 + H_2O \quad (9)$$

$$Fe^{3+} + e^- \rightarrow Fe^{2+},\ E^0 = 0.77V \quad (10)$$

$$Mn^{4+} + e^- \rightarrow Mn^{3+},\ E^0 = 0.95V \quad (11)$$

$$\equiv Mn(IV) + \equiv Fe(II) \rightarrow \equiv Mn(III) + \equiv Fe(III) \quad (12)$$

As discussed above, the results of XPS spectra also indicated that the catalytic activation of PMS is an interfacial reaction, accompanied by metal redox cycles and the generation of free radicals. As a result, multiple bimetallic species were generated in the BFMN nanocomposites, which would form the potential redox cycles for the catalytic reaction. The generated $SO_4^{\bullet-}$ can be further easily converted into $HO^{\bullet}$ by the oxidation of water Eqs. 6 and 7. After that, the central carbon of RhB could be attacked by the generated $HO^{\bullet}$ and $SO_4^{\bullet-}$ (Eq. 9), which could be further degraded by the *N*-de-ethylation process [46] and finally mineralized into CO_2 and H_2O. In a word, the synergy effect in the activation process could mainly originate from the integration of the different functions of Mn and Fe. Mn species acts as the main active site on the catalyst surface, while Fe species acts as the main adsorption site on the reaction matrix.

The above mechanism emphasizes the key role of the entire Mn-O structural unit in BFMN as a PMS to activate the inherent redox center. This means that certain reactions that are generally considered to be thermodynamically unfavorable can be achieved and greatly promoted by optimizing the electronic structure of the catalyst. Another purpose of this study is that the activity of metal catalysts should not be evaluated simply based on the standard redox potential of metal catalysts. Therefore, our research results provide new perspective for guiding the design of efficient catalysts.

Declaration of competing interest

The contents of this manuscript have not been copyrighted or published previously. The authors declare no competing financial interest.

Acknowledgments

This work was supported by the National Key Research and Development Program of China (No. 2020YFC1808300), National Natural Science Foundation of China (Nos. 42077185, 41772264), and the Research Fund of State Key Laboratory of Geohazard Prevention and Geoenvironment Protection (No. SKLGP2020Z002).

Supplementary materials

Supplementary material associated with this article can be found, in the online version, at doi:10.1016/j.cclet.2021.07.063.

References

[1] E. Saputra, S. Muhammad, H. Sun, et al., Appl. Catal. B: Environ. 154 (2014) 246–251.
[2] H. Zhong, M.L. Brusseau, Y. Wang, et al., Water Res. 83 (2015) 104–111.
[3] M.D.F. Hossain, N. Akther, Y. Zhou, Chin. Chem. Lett. 31 (2020) 2525–2538.
[4] R.L. Yin, B.H. Jing, S.X. He, et al., Water Res. 190 (2021) 116720.
[5] J. Li, Y. Li, Z. Xiong, G. Yao, B. Lai, Chin. Chem. Lett. 30 (2019) 2139–2146.
[6] J.L. Yang, M.S. Zhu, D.D. Dionysiou, Water Res. 189 (2021) 116627.
[7] G.X. Huang, C.Y. Wang, C.W. Yang, et al., Environ. Sci. Technol. 51 (2017) 12611–12618.
[8] T. Zhang, H. Zhu, J.P. Croue, Environ. Sci. Technol. 47 (2013) 2784–2791.
[9] Y. Ren, L. Lin, J. Ma, et al., Appl. Catal. B 165 (2015) 572–578.
[10] L. Yu, G. Zhang, C. Liu, et al., ACS Catal. 8 (2018) 1090–1096.
[11] Z. Wan, J. Wang, J. Hazard. Mater. 324 (2017) 653–664.
[12] Q.C. Lin, J.M. Hao, J.H. Li, Chin. Chem. Lett. 17 (2006) 991–994.
[13] H. Zhang, Q. Ji, L. Lai, G. Yao, B. Lai, Chin. Chem. Lett. 30 (2019) 1129–1132.
[14] X. Yan, D. Yue, C. Guo, et al., Chin. Chem. Lett. 31 (2020) 1535–1539.
[15] S. Han, C.B. Mullins, Acc. Chem. Res. 54 (2021) 379–387.
[16] W. Xiang, M. Huang, Y. Wang, et al., Chin. Chem. Lett. 31 (2020) 2831–2834.
[17] J. Hu, H. Dong, J. Qu, Z. Qiang, Water Res. 112 (2017) 1–8.
[18] Y. Wang, H. Sun, H.M. Ang, M.O. Tade, S. Wang, Appl. Catal. B: Environ. 266 (2015) 12–20.
[19] Z.Y. Guo, C.X. Li, M. Gao, et al., Angew. Chem. Int. Ed. 60 (2021) 274–280.
[20] J. Dai, Y.L. Zhu, Y.C. Yin, et al., Small 15 (2019) 1903120.
[21] Y. Chen, S. Lan, M. Zhu, Chin. Chem. Lett. 32 (2020) 2052–2056.
[22] M. Zhang, J. He, Y. Chen, et al., Chin. Chem. Lett. 31 (2020) 2721–2724.
[23] H.J. Cui, H.Z. Huang, B. Yuan, M.L. Fu, Geochem T. 16 (2015) 1-8.
[24] Z.L. Wu, Y.P. Wang, Z.K. Xiong, et al., Appl. Catal. B: Environ. 77 (2020) 119136.
[25] Y.H. Guan, J. Ma, X.C. Li, J.Y. Fang, L.W. Chen, Environ. Sci. Technol. 45 (2011) 9308–9314.
[26] Y. Yang, G. Banerjee, G.W. Brudvig, J.H. Kim, J.J. Pignatello, Environ. Sci. Technol. 2 (2018) 5911–5919.
[27] T.A. Saleh, V.K. Gupta, Colloid Interface Sci. 62 (2011) 337–344.
[28] S. Su, W. Guo, Y. Leng, C. Yi, Z. Ma, J. Hazard. Mater. 244 (2013) 736–742.
[29] X. Jiang, Y.H. Guo, L.B. Zhang, W.J. Jiang, R.Z. Xie, Chem. Eng. J. 341 (2018) 392–401.
[30] S. Zhang, Q. Fan, H. Gao, et al., J. Mater. Chem. A 4 (2016) 1414–1422.
[31] S. Yang, X. Qiu, P. Jin, et al., Chem. Eng. J. 353 (2018) 329–339.
[32] X. Yang, J. Cai, X. Wang, et al., Environ. Sci. Technol. 54 (2020) 3714–3724.
[33] G.S. Timmins, K.J. Liu, E.J.H. Bechara, Y. Kotake, H.M. Swartz, Free Radic. Biol. Med. 27 (1999) 329–333.
[34] Y.H. Jo, S.H. Do, S.H. Kong, Chemosphere 95 (2014) 550–555.
[35] L. Jiang, Q. Ye, J. Chen, Z. Chen, Y. Gu, Colloid Interface Sci. 513 (2018) 748–759.
[36] K. Mishra, T.N. Poudel, N. Basavegowda, Y.R. Lee, J. Catal. 344 (2016) 273–285.
[37] Y. Zhang-Steenwinkel, J. Beckers, A. Bliek, Appl. Catal. A: Gen. 235 (2002) 79–92.
[38] J. Suntivich, H.A. Gasteiger, N. Yabuuchi, et al., Nat. Chem. 3 (2011) 546–550.
[39] T. Wang, Y. Sun, Y. Zhou, et al., ACS Catal. 8 (2018) 8568–8577.
[40] H. Chen, J. He, J. Phys. Chem. C 112 (2008) 17540–17545.
[41] Y. Wang, S. Indrawirawan, X. Duan, et al., Chem. Eng. J. 266 (2015) 12–20.
[42] E. Saputra, S. Muhammad, H. Sun, et al., Appl. Catal. B: Environ. 142 (2013) 729–735.
[43] C. Tan, N. Gao, Y. Deng, et al., J. Hazard. Mater. 276 (2014) 452–460.
[44] J.K. Du, J.G. Bao, Y. Liu, S.H. Kim, D.D. Dionysiou, Chem. Eng. J. 376 (2019) 119193.
[45] Y. Zhou, S. Sun, J. Song, et al., Micro. Nano. Lett. 13 (2018) 572–575.
[46] W. Li, Y. Zhang, P. Zhao, et al., J. Hazard. Mater. 393 (2020) 122399.